VNU Journal of Science: Mathematics – Physics, Vol. 37, No. 3 (2021) 82-92

VNU Journal of Science: Mathematics - Physics

Journal homepage: https://js.vnu.edu.vn/MaP

Original Article

The Resistive Switching Characteristics and Electrical Conduction Mechanisms of Memory Devices Based on Nanocomposite

Doan Thi Tu Uyen[1,2], Le Pham Quynh Nhu Phuong[1,2], Mai Ngoc Xuan Dat[2,3], Pham Kim Ngoc[1,2,*]

[1]*VNU HCM University of Science, 227 Nguyen Van Cu, District 5, Ho Chi Minh City, Vietnam*

[2]*Vietnam National University, Ho Chi Minh City, Vo Truong Toan, Thu Duc, Ho Chi Minh City, Vietnam*

[3]*Center for Innovative Materials and Architectures, Linh Trung, Thu Duc, Ho Chi Minh City, Vietnam*

Received 25 July 2020
Revised 06 November 2020; Accepted 15 December 2020

Abstract: The resistive switching memory device based on nanocomposites has become a potential candidate in the data storage field. Understanding resistive switching characteristics and electrical conduction mechanisms may support the appropriate way to fabricate and control the operation of a device. In this study, a capacitor-like structure using PVA-ZnO as an insulator layer was fabricated by a solution method. The crystalline structure, morphology, and absorption spectrum of ZnO nanoparticles were discussed respectively. The resistive switching effect was observed with the ON/OFF ratio of 0.5×10^2, high endurance, excellent retention and the electrical transport mechanisms were followed by the SCLC and Ohmic's law in the low resistance state and Flower-Nordheim tunneling in the high resistance state. The resistive switching mechanism was contributed by the oxygen vacancies in ZnO nanoparticles and the oxygen ions in the bottom electrode.

Keywords: ZnO nanoparticle, nanocomposite, resistive switching, electrical conduction.

1. Introduction

Nowadays, resistive random access memory (RRAM) is one of the potential research fields promising substitutes for incumbent memories, which have encountered technical and physical

*Corresponding author.
Email address: phamkngoc@hcmus.edu.vn

https//doi.org/ 10.25073/2588-1124/vnumap.4584

limitations [1, 2]. RRAM is a type of non-volatile memory with promising advantages, such as scalability, simple structure, fast operational speed, excellent endurance, long retention, and low power consumption [3]. To further improve the performance of RRAM, switching layers have been developed including inorganic, organic, biological, nanocomposites, and recently hybrid materials [4, 5]. Among these material;s, the hybrid organic-inorganic nanocomposite is a potential candidate because of its ability to combine the advantages both of organic and inorganic components [6].

ZnO, which is an n-type semiconductor with exclusive electro-optical properties, large optical band gap, and good chemical stability, can be synthesized in different morphology such as nanoparticles, nanowire, nanobelts, and nanorods [7]. Wide applications of ZnO such as luminescent material, solar cells, battery, supercapacitors, photocatalysis, biomedical, biosensors piezoelectrics, and optoelectronics. Swapnil et al. reported an RRAM with Ag/ZnO/FTO structure, which has a 10^3 memory window in consecutive 10^2 switching cycles and was stable over 10^2 seconds [8]. Besides, a ZnO-based nonvolatile write-once-read-many-times memory device presented by Toan Thanh Dao et al. had an ON/OFF ratio of 10^4 and retention time of $>10^5$ s [9]. The nanocomposite films of PVA and ZnO have been studied in recent years. The change of the crystalline size of ZnO, the shift in the bandgap, and the position of–OH stretching peak of PVA demonstrate the strong interaction between ZnO nano species and PVA matrix [10]. The nanocomposites of PVA and ZnO are effective in biosensor [11], nonlinear optics [12], photodetectors [13], and food package [14]. Recently, they have been applied in non-volatile resistive switching memory devices [15]. Hmar et al. [15] also reported memory device using ZnO nanoparticles encapsulated in polyvinyl alcohol (PVA) matrix. With the Al/ZnO-PVA/Al device on the flexible PET substrate, the resistive switching effect was achieved with an ON/OFF ratio of 10^1 and a relatively high operating voltage range of -12 ÷12 V. The performance has been improved considerably with the addition of PEDOT:PSS layer.

The electrical conduction, as well as resistive-switching (RS) mechanisms of devices based on nanocomposites, have been reported previously. In hybrid nanocomposites, carrier movement was commonly suggested by suggested Ohmic [7, 16], space charge limited conduction (SCLC) [15, 17], and Fowler-Nordheim tunneling [18], whereas the RS behavior was almost recommended by formation/rupture of metallic or oxygen vacancies filament [6, 15]. Chu et al. [16] introduced a hybrid nanocomposites structure based on ZnO nanorod arrays embedded in insulating polymethyl-methacrylate forming an Al/ZnO–PMMA/ITO structure. The conduction mechanisms at high resistive state (HRS) followed Ohmic conduction while Ohmic and trap-controlled space charge limited conduction (TC-SCLC) was proposed for LRS. The RS mechanism was suggested by trap and de-trap electronics by ionized oxygen vacancy. Similarly, SCLC and Ohmic conduction were assigned LRS and HRS, respectively in another structure using ZnO–PVA/PEDOT:PSS as a switching layer [15]. In their report, the RS mechanisms were suggested by the migration of oxygen ions to form/rupture conduction filament. The forming process was built by gathering rapid pathways of oxygen vacancies created by shifting oxygen ions following the electric field. The rupture process was due to the filling vacancies of oxygen ions under reversed bias.

In this study, we fabricated ZnO nanoparticles and incorporated them into polyvinyl alcohol (PVA), used as a switching layer in the capacitor configuration for RRAM, by a solution method. The incorporation of PVA and ZnO as the active layer may increase the uniform, adhesion, and durable characteristics of a memory device. The Silver/PVA–ZnO/fluorine-doped-tin-oxide showed the reliable and stable bipolar resistive switching (RS) characteristics with 100 cycling endurance in the voltage range of ($-5.5 \rightarrow 4.5$ V) and the RS ratio of 0.5×10^2. Besides, the conduction mechanisms were suggested by the dominance of trap charge limited conduction (SCLC) and Ohmic conduction in low resistance state (LRS) while the current in HRS is controlled by Fowler–Nordheim tunneling. Finally, the RS

mechanism was also proposed due to the migration of electrons through oxygen vacancies within the switching layer under the external electric field.

2. Experiment

Zinc acetate $(CH_3COO)_2Zn$ (Merck, 99,5%) and sodium hydroxide NaOH (Merck, 99.6%) were used as precursors. Firstly, zinc acetate and sodium hydroxide were separately dispersed in a mixture of solvent included deionized water (DI) and ethanol (C_2H_5OH, Merck, 99.8%) (V_{DI}:$V_{ethanol}$ = 2:1) followed by vigorous stirring with the same concentration at 0.55 mol/L. It was maintained for 2 hours to obtain a homogeneous solution. After, NaOH solution was added gradually into zinc acetate solution (V_{NaOH}:$V_{zinc\ acetate}$ = 2:1). Then, it was continuously stirred for 6 hours. Finally, the final mixture was centrifuged and dried to get ZnO nanoparticles.

The configuration of Ag/PVA-ZnO/FTO was studied, which is shown in Figure 1. Firstly, polyvinyl alcohol (PVA – Sigma) was dissolved in DI under continuous stirring for about 2 hours. Then, ZnO nanoparticles were added to incorporate to obtain a homogeneous solution. Then, the PVA-ZnO mixture was covered on FTO commercial substrate by the spin coating process. Finally, the top Ag electrode was deposited by a direct current sputtering technique.

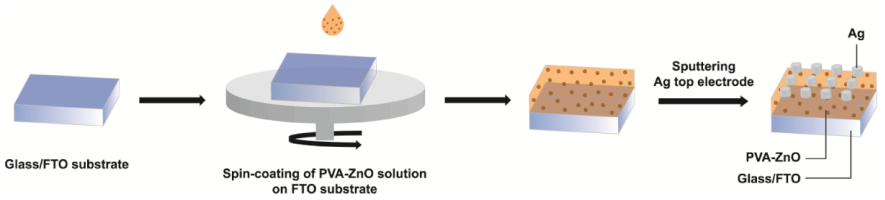

Figure 1. Schematic representation of the fabrication process of the memory device.

The structure of the prepared ZnO Nps was analyzed by Bruker D8 Advance X-ray diffractometer (XRD) with Cu-Kα radiation (λ = 0.154 nm). The Fourier transform-infrared spectroscopy (4800S spectrometer FTIR (Shimadzu Corporation) was used to study vibration characteristics in the mid-infrared range from 400 to 3900 cm^{-1}. The morphology features and distribution of ZnO were estimated by Scanning Electron Microscope (SEM, S4800, Hitachi, Japan) and Transmission Electron Microscope (TEM, JEM - 1400, JEOL, Japan). The room temperature photoluminescence (PL) emission spectra were recorded on a spectrophotometer (Horiba Jobin Yvon IHR) using a 325 nm of He-Cd laser as an excitation source. The absorption spectra were executed by V730 (Jasco) in the UV-vis range. Finally, the current-voltage (I–V) characteristics (Keithley 2400) of the Ag/PVA–ZnO/FTO memory device were employed by applying a DC voltage continuously with the bottom electrode (FTO), which is biased, while the top one (Ag) is grounded.

3. Result and Discussion

3.1. Structural Characteristics

The XRD result of ZnO nanoparticles was studied to determine the crystalline structure, which is shown in Figure 1 (a). The data was recorded by using Cu Kα radiation (1.5406 Å) in a range of 2θ from 10° to 80°. All peaks were observed clearly at 31.7°, 34.5°, 36.2°, 47.6°, 56.5°, 62.9°, 66.5°, 67.9°, 69.0°, 72.7°, 77.0° corresponding to characteristic indexing planes (100), (002), (101), (102), (110),

(103), (200), (112), (201), (004) and (202), respectively. The most intense peaks were at (100), (002), and (101) planes. It indicated the hexagonal wurtzite crystal structure of ZnO nanoparticles, which was confirmed by previous reports [19, 20]. In the XRD pattern, no diffraction peaks from other types were recorded, verifying that all precursors had been extruded completely, implying the high purity of the synthesized products.

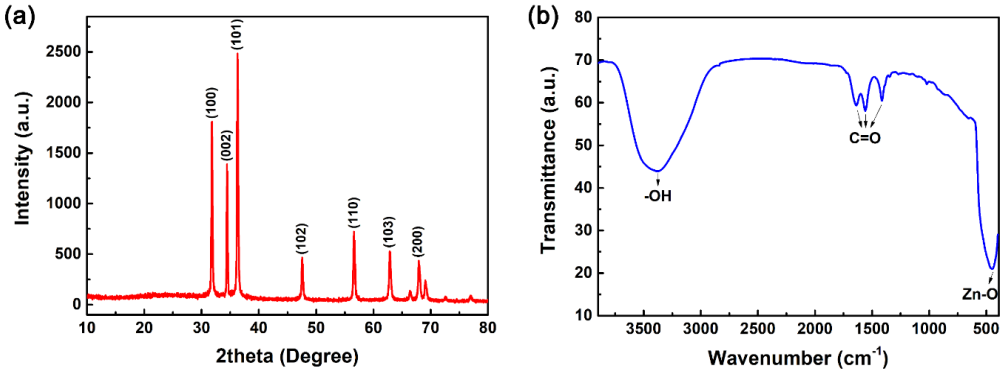

Figure 2. (a) XRD pattern and (b) FTIR spectrum of ZnO nanoparticles.

The FTIR spectroscopy evaluated the characteristic vibration of ZnO nanoparticles in a range from 400 to 3900 cm^{-1} (Figure 2b). At around 450 cm^{-1}, a broad strong peak was recorded corresponding to the stretching vibration of Zn–O bonds [20, 21]. The broad band was observed from 3000 to 3600 cm^{-1}, assigned for free O–H stretching and deformation vibrations. Besides, the bands at 1406 cm^{-1}, 1562 cm^{-1} were attributed for C=O asymmetric vibration while an asymmetric C=O oscillation appeared at 1647 cm^{-1} [22].

3.2. Surface Morphology

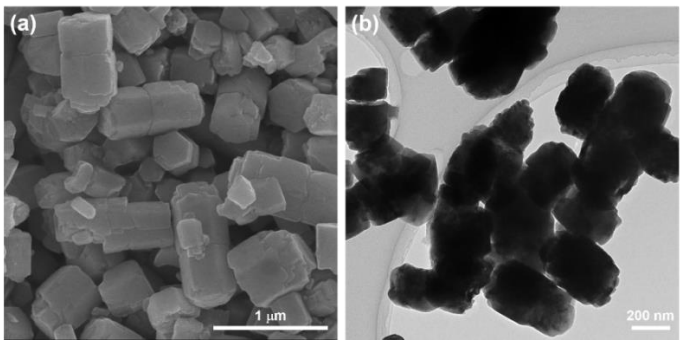

Figure 3. (a) SEM and (b) TEM images of ZnO nanoparticles.

The morphology features and distribution of synthesized ZnO nanoparticles were estimated by SEM and TEM images, as shown in Figure 3. The SEM image revealed the hexagonal-rode-like morphology with the diversity of dimensions of ZnO nanoparticles in the range from 50 to 200 nm. The nanoparticles have been grain boundary, relatively separated from each other. Besides, the TEM has also confirmed

the morphology of the nanoparticles as in SEM. From morphology, ZnO nanoparticles showed a high crystal structure with hexagonal-rode like morphology.

3.3. Absorption Spectroscopy

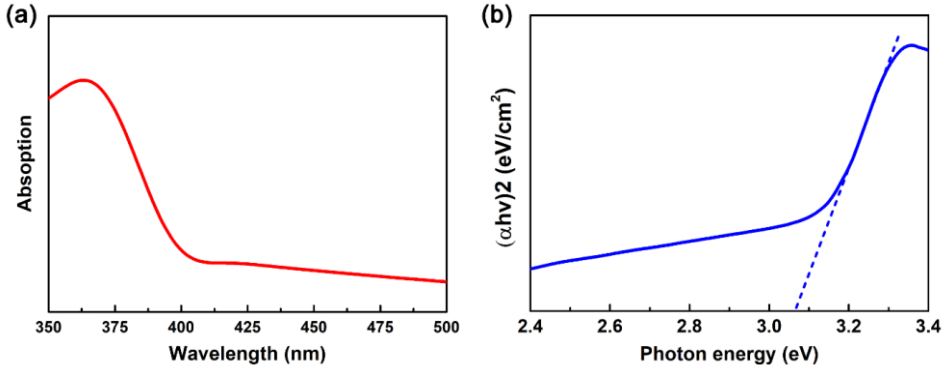

Figure 4. (a) Absorption spectrum and (b) Optical bandgap energy from the Tauc plot of ZnO nanoparticles.

The room temperature absorption spectra and corresponding optical bandgap energies of ZnO nanoparticles are shown in Figure 4. The spectrum reveales a characteristic sharp absorption peak of ZnO nanoparticles at around 372 nm. The direct bandgap energy (E_g) for the nanoparticles is determined by fitting the reflection data to the direct transition equation $(\alpha h\nu)^2 = k\,(h\nu - E_g)$ where α is the optical absorption coefficient, $h\nu$ is the photon energy, E_g is the direct bandgap [23]. Plotting $(\alpha h\nu)^2$ as a function of photon energy and extrapolating the linear portion of the curve to absorption equal to zero gives the value of the direct bandgap to be 3.08 eV. This value was lower than 3.3 eV of zinc oxide bulk [24]. This redshift of the bandgap energy might be due to the agglomeration of the nanocrystallites into larger crystallites or due to the defects in materials [25].

3.4. Photoluminescence (PL) Analysis

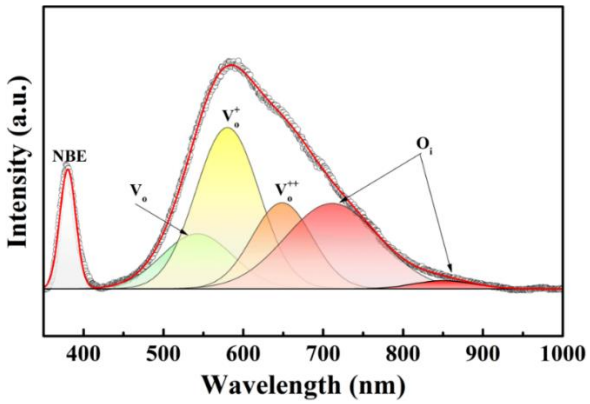

Figure 5. PL spectrum of ZnO NPs at room temperature.

To determine the quality and the presence of defects in the ZnO NPs, the photoluminescence (PL) spectroscopy was used. Figure 5 shows the normalized PL spectrum of the ZnO NPs at room

temperature. Fundamentally, the PL peak in the UV region is associated with the band-to-band emission while the visible emission originates from the defect levels [26]. As seen in Figure 5, the PL spectra of ZnO NPs exhibit a UV emission band centered at about 387 nm (3.2 eV) and a broad emission peak at a visible region of about 600 nm (2.06 eV). In our study, the bandgap of ZnO NPs (3.2 eV) was smaller than the bandgap of ZnO bulk (3.3 eV) [24]. This decrease may be the high defect concentration including oxygen vacancies, interstitial and lattice defects which were existing in nanomaterials. The bandgap value examined by PL analysis was slightly different from the value calculated by the absorption spectrum because of the nature of the analyzed technique.

The broad visible emission peak could be deconvoluted into five peaks which are neutral oxygen vacancies (V_O) at 542 nm, oxygen vacancies with a single charge (V_O^+) at 580 nm, oxygen vacancies double charge (V_O^{++}) at 648 nm, and oxygen interstitials (O_i) at 711 and 850 nm. The green emission was originated by the transition from the conduction band to the deep levels of oxygen vacancies of V_O (520–570 nm) [27]. The yellow emission might be due to V_O^+ (570–620 nm) and V_O^{++} (620–670 nm) [28]. The orange emission (670–720 nm) was attributed to the transition from the conduction band to the O_i level [29], while the red emission (720 -780 nm) was the original transition from Zn_i to O_i [30]. The existing defects in ZnO NPs might influence significantly the charge transport process and resistive switching behavior of memory devices.

3.5. Resistive switching of the memory device

The current-voltage (I–V) curves of the Ag/PVA/FTO and Ag/PVA–ZnO/FTO devices are shown in Figure 6 (a) and 6 (b), respectively. The bottom electrode (FTO) is biased while the top one (Ag) is grounded during repeatedly cycling sweeps in the voltage range from - 5.5 V to 4.5 V. In the Ag/PVA/FTO device, there is no hysteresis in the I–V curve or no resistive switching effect (Figure 6(a)). On the contrary, the Ag/PVA–ZnO/FTO device shows a non-volatile counter-clockwise bipolar resistive switching behavior in which the SET process is regarded the positive electric field and the RESET is the reverse one (Figure 6(b)). It is indicated that the memory effect of the device was influenced significantly by embedding ZnO NPs. An as-prepared device was at high resistance state (HRS) about 10-4 A. By sweeping the positive voltage from zero to 4.5 V, the initial state of the device switched from HRS into the low resistance state (LRS) around 10-1 A at ~1 V (VSET). This process was corresponding to the writing process in memory. The LRS of the device remained until the reversed bias applied from zero to –5.5 V. This process makes the current structure decrease gently back to HRS, leading to the reset or erase process. The device showed a bipolar resistive switching effect under the external electric field.

To provide a further understanding of the performance of this device, the evolutions of the resistances at HRS and LRS under a voltage of 0.5 V in the endurance test and the cumulative probability of resistances were investigated as shown in Figure 6 (c) and Figure 6 (d), respectively. The variation of HRS and LRS during sweeping cycles is relatively small. Also, the ON/OFF resistance ratio is an average of 0.5×102. Figure 5 (e) exhibits the retention test at HRS and LRS states. The performance stability or retention characteristic of the memory device is one of the important parameters for practical applications. It was tested by applying a constant voltage of 0.5 V and measuring current (or resistance) vs. time separately in the LRS and the HRS. From Figure 6 (e), it is observed that the resistance values of the device at the HRS and LRS states remain almost constant of ~ 0.4×102 Ω and ~1.5×103 Ω over 104 s. There was no noticeable degradation of resistances in both the HRS and LRS states which showed the excellent retention characteristic of the memory device. The histogram of the SET and RESET voltage of the memory device as shown in Figure 6 (f). A narrow distribution of VSET (~ +1 V) and

VRESET (~ – 4 V) was obtained in our device. About 3 V differences of two threshold switching voltages were observed between LRS and HRS, suggesting a clear identification between the two writing/erasing states.

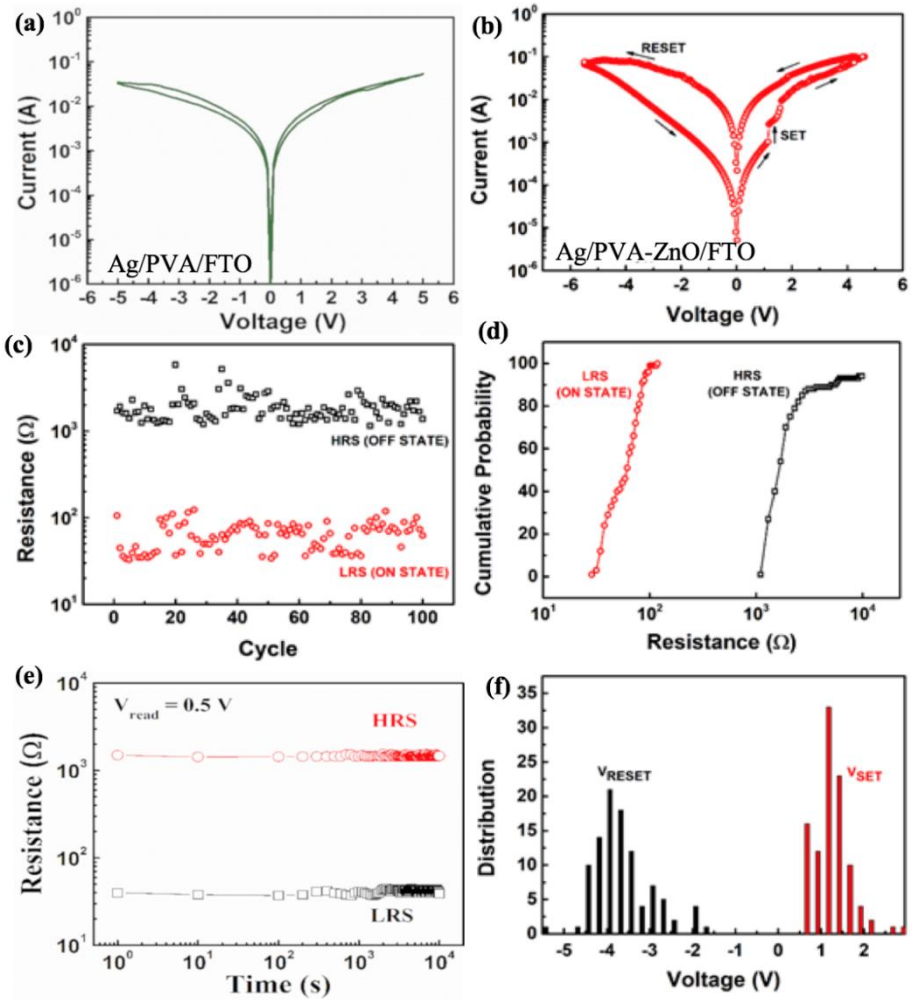

Figure 6. Current – Voltage (I–V) characteristics of (a) Ag/PVA/FTO and (b) Ag/PVA–ZnO/FTO devices, (c) Endurance test during 100 cycles, (d) Cumulative Probability of Resistance at HRS and LRS states, (d) Retention time at HRS and LRS states and (f) Distribution of Operation Voltages of Ag/PVA-ZnO/FTO device.

3.6. Electrical Conduction and Resistive Switching Mechanisms

To investigate the conduction mechanism as well as the resistive switching mechanism which was occurred within the PVA–ZnO switching layer, the I-V characteristic of the Ag/PVA–ZnO/FTO device was fitted following to appropriate mechanism (Figure7 (b-d)). In the first sweep from 0 V to 4.5 V, the current is increased following the voltage in distinct regimes. The current increases following the voltage with the slope of ~ 1.35 which is larger than the slope of Ohmic conduction ($I \alpha V$) in the small electric field [31]. At V_{SET} of ~1.13 V, the current is increased more abruptly than the previous voltage with the slope of 10.8 which is inherent to the trap-fill-limit region ($I \alpha V^n$, $n > 3$) [32], indicating the switch from HRS to LRS, activating the device to ON state. Afterward, the current is continually increased

with the slope of 1.98 before the second SET at the voltage of 1.57 V; however, this process was not referred to the first SET. The current was retained at LRS until the end of the first sweep from 4.5 V to 0 V with the slope of 2.11 (Child's law region – $I \alpha V^2$) [33] and even in the backward of voltage with the slope of 1.09, respectively. According to the J-E curve in Figure 7b, the slope of the first two stages is relatively consistent with the trapped charge limited conduction (SCLC) and Ohmic conduction, corresponding to the LRS of the device. When negative biasing on the bottom electrode, the pristine current was still in the LRS with a slope of 1.06 adhering to Ohmic conduction (Figure 7 (c)). In the final stage of the voltage sweep, the correlative plot of $Ln(J/E^2) \alpha 1/E$ shows a large negative slope with a crowd data points in the high electric field region as shown in Figure 7 (d), revealing that the current in HRS is controlled by Fowler-Nordheim tunneling [31].

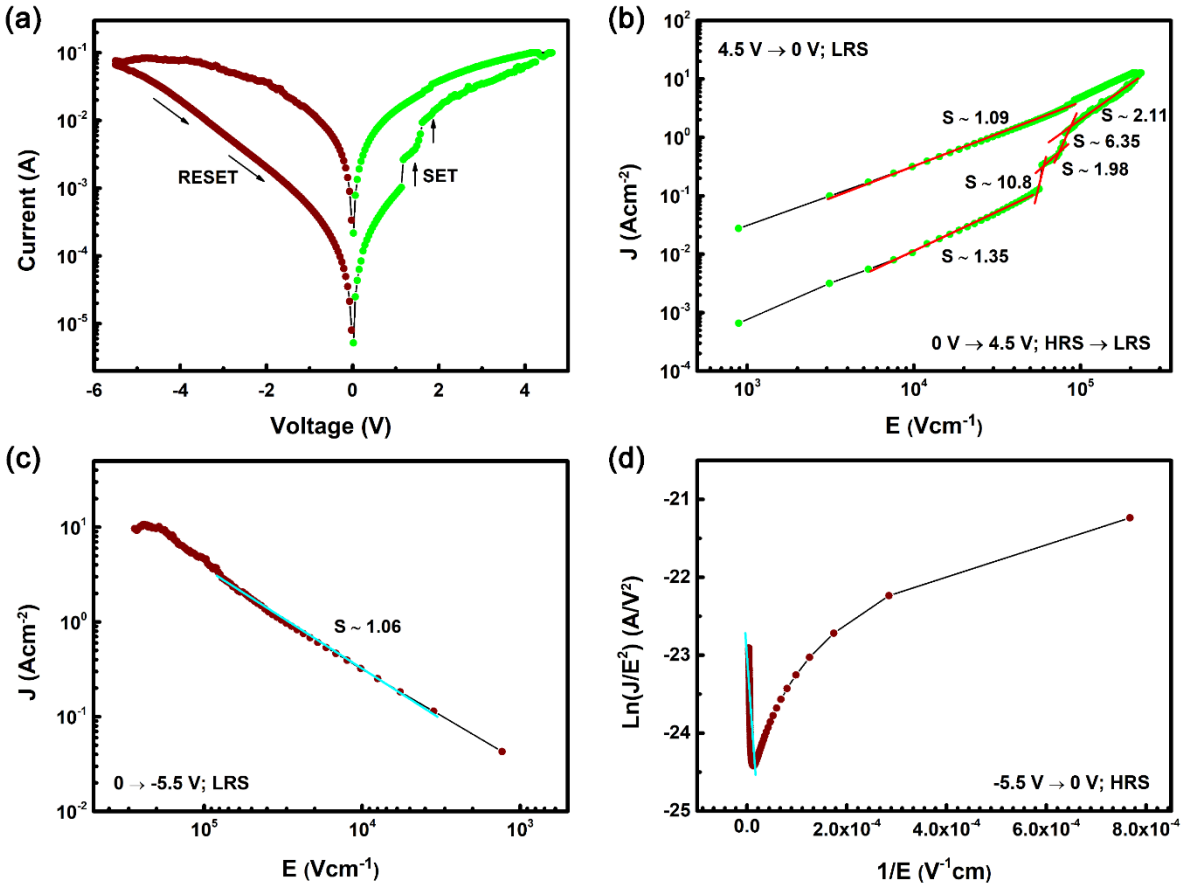

Figure 7. (a) The I–V characteristic of Ag/PVA–ZnO/FTO plotted in double-logarithmic scale; Relation of J – E for the voltage (b) from 0 V to 4.5 V and vice versa, (c) from 0 V to -5.5 V; Relation of $Ln(J/E^2)$ – 1/E for the negative voltage from -5.5 V to 0 V.

Based on the I–V characteristic and electrical conduction mechanism of the memory device, we propose that the resistive switching in Ag/PVA–ZnO/FTO device is due to the migration of electrons through oxygen vacancies within the switching layer under the external electric field. When the negative voltage was applied to the top electrode (Ag), the electrons were injected from Ag into PVA–ZnO dielectric film through thermionic emission. In the PVA–ZnO layer, abundant oxygen vacancies existed

in ZnO NPs (from PL spectrum) which acted like trap centers in the PVA matrix. The conduction mechanism in this stage was related to SCLC model as in Figure 7(b). In addition, the accumulation of ZnO NPs can be the reason for diminishing the distance between oxygen vacancies and helps the electrons transport via trap easily. After filling all the traps, the subsequently injected electrons could move directly through the PVA–ZnO thin film toward to FTO electrode within Ohmic conduction and switch the device to ON state.

Particularly, the FTO bottom electrode acted as a reservoir source of ion oxygens [34]. In the reversed bias, therefore, oxygen vacancies in the FTO/ PVA–ZnO interface were partially occupied by ion oxygens whichcame from the FTO electrode. As a result, the electrons could not migrate through the PVA–ZnO film because of the lack of oxygen vacancies which were filled by oxygen ions. This interruption of electron transport caused the drop of current and turned the device back to the OFF state. In Ag/PVA–ZnO/FTO device, oxygen vacancies in ZnO NPs played a crucial important role in the management of the resistive switching mechanism. The Ag/PVA/FTO device (without ZnO NPs) has the absence of a resistive switching effect. The influence of oxygen vacancies in the resistive switching mechanism has also been reported in some other studies [35]–[37].

4. Conclusion

In summary, we successfully fabricated ZnO nanoparticles as well as RRAM devices using PVA–ZnO as an RS layer in Ag/PVA–ZnO/FTO structure. Structural results indicated high crystalline of obtained ZnO nanoparticles and hexagonal-rode like morphology. Besides, these devices showed the bipolar resistive-switching characteristic with the ON/OFF ratio around 0.5×10^2 and highly stable endurance. The conduction mechanisms were suggested by the dominance of trap charge limited conduction (SCLC) and Ohmic conduction in low resistance state (LRS) while the current in HRS was controlled by Fowler–Nordheim tunneling. Finally, the RS mechanism was also proposed due to the migration of electrons through oxygen vacancies within the switching layer under the external electric field.

Acknowledgments

This work was financially supported by the Vietnam National Foundation for Science and Technology Development (NAFOSTED) under Grant 103.02-2018.67.

References

[1] T. C. Chang, F. Y. Jian, S. C. Chen, And Y. T. Tsai, Developments In Nanocrystal Memory, Mater. Today, Vol. 14, No. 12, 2011, pp. 608–615, https://doi.org/10.1016/S1369-7021(11)70302-9.

[2] M. F. Hung, Y. C. Wu, J. J. Chang, And K. S. Chang-Liao, Twin Thin-Film Transistor Nonvolatile Memory With An Indium-Gallium-Zinc- Oxide Floating Gate, Ieee Electron Device Lett., Vol. 34, No. 1, 2013, pp. 75–77, https://doi.org/10.1109/LED.2012.2226232.

[3] P. Misra, A. K. Das, And L. M. Kukreja, Switching Characteristics Of ZnO Based Transparent Resistive Random Access Memory Devices Grown By Pulsed Laser Deposition, Phys. Status Solidi Curr. Top. Solid State Phys., Vol. 7, No. 6, 2010, pp. 1718–1720, https://doi.org/10.1002/pssc.200983244.

[4] N. Raeis-Hosseini And J. S. Lee, Resistive Switching Memory Using Biomaterials, J. Electroceramics, Vol. 39, 2017, pp. 223–238, https://doi.org/10.1007/s10832-017-0104-z.

[5] Y. Song Et Al., 1/f Noise Scaling Analysis In Unipolar-Type Organic Nanocomposite Resistive Memory, Acs Nano, Vol. 9, No. 7, 2015, pp. 7697–7703, https://doi.org/10.1021/acsnano.5b03168.

[6] G. Casula Et Al., Air-Stable, Non-Volatile Resistive Memory Based On Hybrid Organic/Inorganic Nanocomposites, Org. Electron., Vol. 18, 2015, pp. 17–23, https://doi.org/10.1016/j.orgel.2015.01.001.

[7] G. Khurana, P. Misra, N. Kumar, And R. S. Katiyar, Tunable Power Switching In Nonvolatile Flexible Memory Devices Based On Graphene Oxide Embedded With ZnO Nanorods, J. Phys. Chem. C, Vol. 118, 2014, pp. 21357–21364, https://doi.org/10.1021/jp506856f.

[8] S. R. Patil Et Al., Solution-Processable ZnO Thin Film Memristive Device For Resistive Random Access Memory Application, Electron., Vol. 7, No. 12, 2018, pp. 445, https://doi.org/10.3390/electronics7120445.

[9] T. Thanh Dao Et Al., High-Performance Nonvolatile Write-Once-Read-Many-Times Memory Devices With ZnO Nanoparticles Embedded In Polymethylmethacrylate, Appl. Phys. Lett., Vol. 99, No. 23, 2011, pp. 233303, https://doi.org/10.1063/1.3665937.

[10] M. Aslam, M. A. Kalyar, And Z. A. Raza, Polyvinyl Alcohol: A Review Of Research Status And Use Of Polyvinyl Alcohol Based Nanocomposites, Polymer Engineering And Science, Vol. 58, No. 12, 2018, pp. 2119–2132, https://doi.org/10.1002/pen.24855.

[11] N. K. Sekar Et Al., Fabrication Of Electrochemical Biosensor With ZnO-PVA Nanocomposite Interface For The Detection Of Hydrogen Peroxide, J. Nanosci. Nanotechnol., Vol. 18, No. 6, 2017, pp. 4371–4379, https://doi.org/10.1166/jnn.2018.15259.

[12] V. Viswanath, S. S. Nair, G. Subodh, And C. I. Muneera, Zinc Oxide Encapsulated Poly (Vinyl Alcohol) Nanocomposite Films As An Efficient Third-Order Nonlinear Optical Material: Structure, Microstructure, Emission And Intense Low Threshold Optical Limiting Properties, Mater. Res. Bull., Vol. 112, 2019, pp. 281–291, https://doi.org/10.1016/j.materresbull.2018.12.022.

[13] S. S. Mousavi, B. Sajad, And M. H. Majlesara, Fast Response ZnO/PVA Nanocomposite-Based Photodiodes Modified By Graphene Quantum Dots, Mater. Des., Vol. 162, 2019, pp. 249–255, https://doi.org/10.1016/j.matdes.2018.11.037.

[14] E. Gharoy Ahangar, M. H. Abbaspour-Fard, N. Shahtahmassebi, M. Khojastehpour, And P. Maddahi, Preparation and Characterization Of PVA/ZnO Nanocomposite, J. Food Process. Preserv., Vol. 39, No. 6, 2015, pp. 1442–1451, https://doi.org/10.1111/jfpp.12363.

[15] J. J. L. Hmar, Flexible Resistive Switching Bistable Memory Devices Using ZnO Nanoparticles Embedded In Polyvinyl Alcohol (PVA) Matrix And Poly(3,4-Ethylenedioxythiophene) Polystyrene Sulfonate (Pedot:PSS), Rsc Adv., Vol. 8, No. 36, 2018, pp. 20423–20433, https://doi.org/10.1039/C8RA04582H.

[16] Z. L. Tseng, P. C. Kao, M. F. Shih, H. H. Huang, J. Y. Wang, And S. Y. Chu, Electrical Bistability In Hybrid ZnO Nanorod/Polymethylmethacrylate Heterostructures, Appl. Phys. Lett., Vol. 97, No. 21, 2010, pp. 212103, https://doi.org/10.1063/1.3511756.

[17] N. K. Pham Et Al., Comprehensive Resistive Switching Behavior Of Hybrid Polyvinyl Alcohol And Tio 2 Nanotube Nanocomposites Identified By Combining Experimental And Density Functional Theory Studies, J. Mater. Chem. C, Vol. 6, No. 8, 2018, pp. 1971–1979, https://doi.org/10.1039/C7TC05140A.

[18] D. I. Son, C. H. You, W. T. Kim, J. H. Jung, And T. W. Kim, Electrical Bistabilities And Memory Mechanisms Of Organic Bistable Devices Based On Colloidal ZnO Quantum Dot-Polymethylmethacrylate Polymer Nanocomposites, Appl. Phys. Lett., Vol. 94, No. 13, 2009, pp. 35–38, https://doi.org/10.1063/1.3111445.

[19] R. Viswanatha Et Al., Synthesis And Characterization Of Mn-Doped ZnO Nanocrystals, J. Phys. Chem. B, Vol. 108, No. 20, 2004, pp. 6303–6310, https://doi.org/10.1021/jp049960o.

[20] Y. Song And J. Yang, Preparation And In-Vitro Cytotoxicity Of Zinc Oxide Nanoparticles Against Osteoarthritic Chondrocytes, Trop. J. Pharm. Res., Vol. 15, No. 11, 2016, pp. 2321–2327, https://doi.org/10.4314/tjpr.v15i11.4.

[21] A. Khorsand Zak, R. Razali, W. H. Abd Majid, And M. Darroudi, Synthesis And Characterization Of A Narrow Size Distribution Of Zinc Oxide Nanoparticles, Int. J. Nanomedicine, Vol. 6, No. 1, 2011, pp. 1399–1403, https://doi.org/10.2147/IJN.S19693.

[22] P. Rajiv, S. Rajeshwari, And R. Venckatesh, Bio-Fabrication Of Zinc Oxide Nanoparticles Using Leaf Extract of Parthenium Hysterophorus L. And Its Size-Dependent Antifungal Activity Against Plant Fungal Pathogens, Spectrochim. Acta - Part A Mol. Biomol. Spectrosc., Vol. 112, 2013, pp. 384–387, https://doi.org/10.1016/j.saa.2013.04.072.

[23] S. S. M, L. Bose, And G. Kc, Optical Properties Of ZnO Nanoparticles, Sb Acad. Rev., Vol. Xvi, No. 1, 2009, pp. 57–65.

[24] K. S. Hemalatha, K. Rukmani, N. Suriyamurthy, And B. M. Nagabhushana, Synthesis, Characterization And Optical Properties Of Hybrid PVA-ZnO Nanocomposite: A Composition Dependent Study, Mater. Res. Bull., Vol. 51, 2014, pp. 438–446, https://doi.org/10.1016/j.materresbull.2013.12.055.

[25] N. Rana, A. K. Gathania, And S. Chand, Structural And Optical Properties Of ZnO Nanoparticles, International Conference on Solid-State And Organic Lighting, 2014, Vol. 6, pp. 8–12.

[26] M. C. Jun, S. U. Park, And J. H. Koh, Comparative Studies Of Al-Doped ZnO And Gadoped ZnO Transparent Conducting Oxide Thin Films, Nanoscale Res. Lett., Vol. 7, 2012, pp. 1–6, https://doi.org/10.1186/1556-276X-7-639.

[27] J. Li, S. Srinivasan, G. N. He, J. Y. Kang, S. T. Wu, And F. A. Ponce, Synthesis And Luminescence Properties Of ZnO Nanostructures Produced By The Sol-Gel Method, J. Cryst. Growth, Vol. 310, No. 3, 2008, pp. 599–603, https://doi.org/10.1016/j.jcrysgro.2007.11.054.

[28] K. Bandopadhyay And J. Mitra, Zn Interstitials And O Vacancies Responsible For N-Type ZnO: What Do The Emission Spectra Reveal?, Rsc Adv., Vol. 5, No. 30, 2015, pp. 23540–23547, https://doi.org/10.1039/C5RA00355E.

[29] D. Alegre, M. S. Martín-González, B. Alén, O. Caballero-Calero, And C. V. Manzano, Synthesis And Luminescence Properties Of Electrodeposited ZnO Films, J. Appl. Phys., Vol. 110, No. 4, 2011, pp. 043538, https://doi.org/10.1063/1.3622627.

[30] C. T. Quy Et Al., C_2H_5OH And NO_2 Sensing Properties Of ZnO Nanostructures: Correlation Between Crystal Size, Defect Level And Sensing Performance, Rsc Adv., Vol. 8, No. 10, 2018, pp. 5629–5639, https://doi.org/10.1039/C7RA13702H.

[31] E. W. Lim And R. Ismail, Conduction Mechanism Of Valence Change Resistive Switching Memory: A Survey, Electronics, Vol. 4, No. 3, 2015, pp. 586–613, https://doi.org/10.3390/electronics4030586.

[32] G. Zhou, Z. Ren, L. Wang, B. Sun, S. Duan, And Q. Song, Artificial And Wearable Albumen Protein Memristor Arrays With Integrated Memory Logic Gate Functionality, Mater. Horizons, Vol. 6, No. 9, 2019, pp. 1877–1882, https://doi.org/10.1039/C9MH00468H.

[33] A. Younis, D. Chu, And S. Li, Bi-Stable Resistive Switching Characteristics In Ti-Doped ZnO Thin Films, Nanoscale Res Lett., Vol. 8, No. 1, 2013, pp. 1–6, https://doi.org/10.1186/1556-276X-8-154.

[34] C. Kumari, I. Varun, S. P. Tiwari, And A. Dixit, Interfacial Layer Assisted, Forming Free, And Reliable Bipolar Resistive Switching In Solution Processed $BiFeO_3$ Thin Films, Aip Adv., Vol. 10, No. 2, 2020, https://doi.org/10.1063/1.5134972.

[35] S. Bhattacharjee, P. K. Sarkar, N. Roy, And A. Roy, Improvement Of Reliability Of Polymer Nanocomposite Based Transparent Memory Device By Oxygen Vacancy Rich ZnO Nanorods, Microelectron. Eng., Vol. 164, 2016, pp. 53–58, https://doi.org/10.1016/j.mee.2016.04.027.

[36] A. Chiolerio, I. Roppolo, K. Bejtka, A. Asvarov, And C. F. Pirri, Resistive Hysteresis In Flexible Nanocomposites And Colloidal Suspensions: Interfacial Coupling Mechanism Unveiled, Rsc Adv., Vol. 6, No. 61, 2016, pp. 56661–56667, https://doi.org/10.1039/C6RA10503C.

[37] C. Hu Et Al., The Effect Of Oxygen Vacancy On Switching Mechanism Of ZnO Resistive Switching Memory, Appl. Phys. Lett., Vol. 110, No. 7, 2017, pp. 1–5, https://doi.org/10.1063/1.4976512.